Scripta Materialia 236 (2023) 115666

Contents lists available at ScienceDirect

Scripta Materialia

journal homepage: www.journals.elsevier.com/scripta-materialia

Ultra-fine microstructure and exceptional low coercivity developed in a high-B_s Fe-Si-B-P alloy by co-alloying Ni, Mo, and Cu

Fayuan Shen [a,b], Bowen Zang [b,*], Lijian Song [b], Juntao Huo [b,c], Yan Zhang [a], Jun-Qiang Wang [b,c,*]

[a] School of Materials Science and Engineering, Zhejiang University of Technology, Hangzhou 310014, China
[b] CAS Key Laboratory of Magnetic Materials and Devices, and Zhejiang Province Key Laboratory of Magnetic Materials and Application Technology, Ningbo Institute of Materials Technology and Engineering, Chinese Academy of Sciences, Ningbo 315201, China
[c] Center of Materials Science and Optoelectronics Engineering, University of Chinese Academy of Sciences, Beijing 100049, China

ARTICLE INFO

Keywords:
Nanocrystalline alloy
Soft magnet
High saturation magnetic induction
Micro-alloying
Microstructure refinement

ABSTRACT

Designing soft magnetic alloys with high saturation magnetic induction (B_s) is of great importance for improving the power density of electric and electronic devices. For high-B_s nanocrystalline alloys, the main problem is the grain coarsening effect induced by high Fe content (>80 at.%), which deteriorates the soft magnetic properties. In present work, we designed new Fe-based nanocrystalline alloys by microalloying a Fe-Si-B-P alloy. The co-alloying of Ni, Mo, and Cu effectively refines the microstructure of nanocrystalline alloys from 28.5 nm to 13.1 nm and increased the stability of soft magnetic properties. Even though there are 28-nm-large surface crystallites in the amorphous precursors, an exceptional low coercivity of 1–2 A/m with a high B_s of 1.81 T was developed after nanocrystallization. These excellent magnetic properties could be maintained within a wide annealing temperature window of 50 K and an annealing time window up to 600 s for high heating rate annealing.

Developing superior soft magnetic materials is of great importance for the increasingly electrified world. Fe-based nanocrystalline soft magnetic alloys have attracted great interests due to their advantages in developing devices with both high power density and high energy efficiency [1–9]. Their excellent soft magnetic properties are from the ultra-fine microstructure developed from amorphous precursors [10–12]. Increasing the saturation magnetic induction (B_s) of soft magnetic materials could increase the power density of the relevant products, which is critical for the miniaturization of devices. A high-B_s nanocrystalline soft magnetic alloy often requires a high Fe-content and the least amount of early transition metals (ETMs), while enough Cu addition is necessary for maintaining the good magnetic softness (i.e., low coercivity, high permeability, low core loss, etc.) [13–15]. All these requisites reduce the glass-forming ability (GFA) of Fe-based nanocrystalline alloys. The resultant poor quality of amorphous precursors leads to coarse microstructure after crystallization, and hence deteriorates the soft magnetic properties. In present, this is one of the main hinderance to the development of high-B_s nanocrystalline soft magnetic alloys.

Increasing heating rate could effectively improve the soft magnetic properties of high-B_s Fe-based nanocrystalline alloys [16–20]. The high crystallization temperature and high relaxation temperature achieved by increasing heating rate promote the nucleation kinetics in Fe-based amorphous alloys [21,22]. Continuous production of Fe-based nanocrystalline alloys by high heating rate annealing technique is accessible [19], but the narrow processing temperature and time window, e.g., ~20 K and ≤ 20 s, are potential difficulties for industrial application [23,24]. Designing new nanocrystalline alloys with good soft magnetic properties as well as wide processing window for high heating rate annealing would greatly boost the application of high-B_s Fe-based nanocrystalline alloys.

In this work, a new nanocrystalline soft magnetic alloy is designed by microalloying Ni, Mo, and Cu to a $Fe_{84}Si_4B_{8.4}P_{3.6}$ alloy. The nanocrystalline $Fe_{84-x-z}Si_{3.6-y}B_{8.4}P_{3.6}Ni_xMo_yCu_z$ alloys processed by a rapid annealing method was characterized. The variation of their coercivity and saturation magnetic induction versus isothermal annealing temperature and isothermal annealing time was investigated.

Fe-Si-B-P-(Ni-Mo-Cu) alloy ingots were prepared by induction

* Corresponding authors.
E-mail addresses: zangbowen@nimte.ac.cn (B. Zang), jqwang@nimte.ac.cn (J.-Q. Wang).

https://doi.org/10.1016/j.scriptamat.2023.115666
Received 17 April 2023; Received in revised form 16 June 2023; Accepted 11 July 2023
Available online 24 July 2023

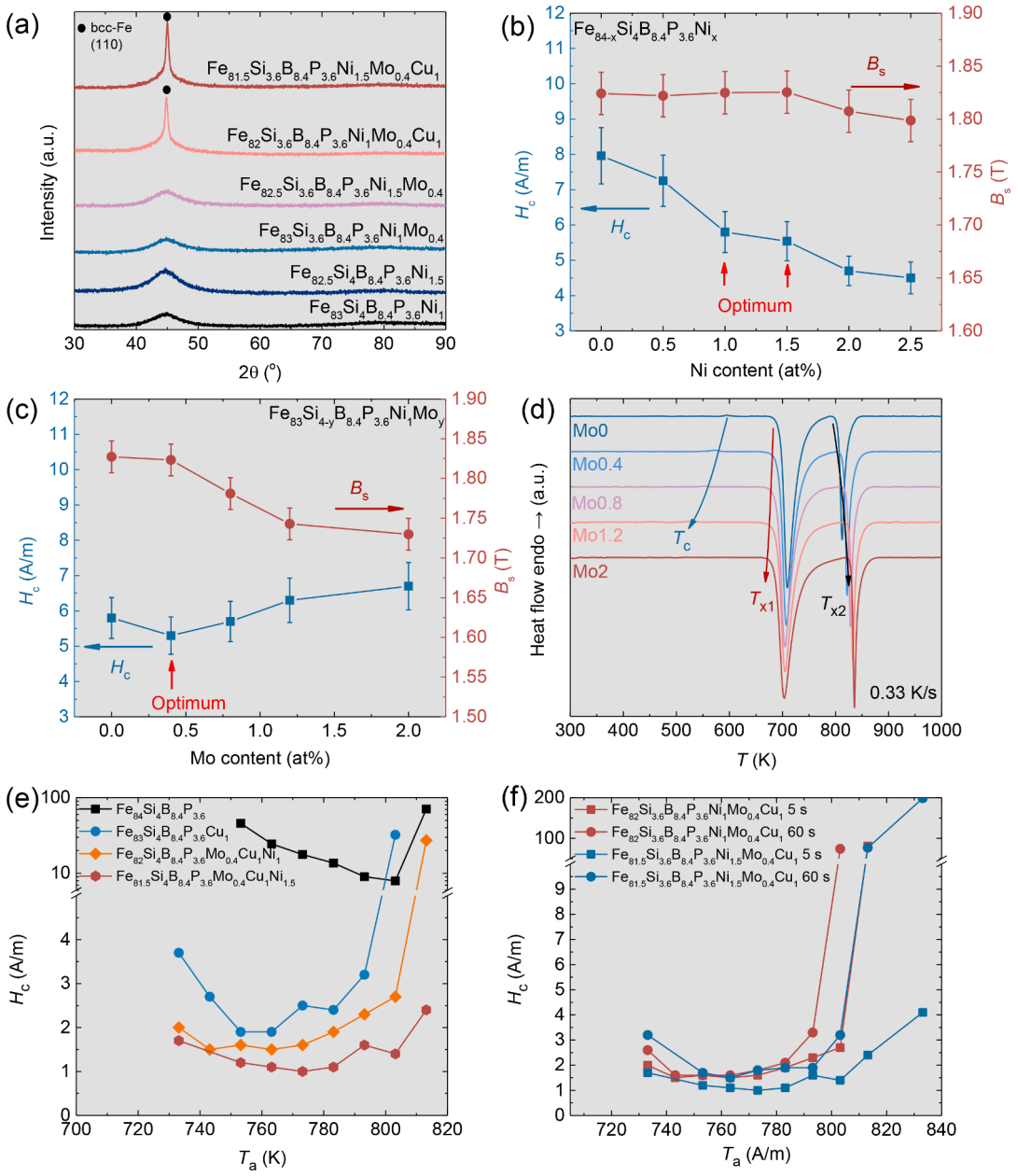

Fig. 1. (a) XRD patterns of as-spun ribbons acquired from their free side (b) The H_c and B_s of optimally annealed $Fe_{84-x}Si_4B_{8.4}P_{3.6}Ni_x$ alloys with $x = 0 – 2.5$; (c) The H_c and B_s of optimally annealed $Fe_{83}Si_{4-y}B_{8.4}P_{3.6}Ni_1Mo_y$ alloys with $y = 0 – 2$; (d) The isochronal DSC curves of as-spun $Fe_{84-x}Si_{4-y}B_{8.4}P_{3.6}Ni_xMo_y$ alloys; (e) The H_c vs. T_a plot of nanocrystalline $Fe_{82-x-z}Si_{4-y}B_{8.4}P_{3.6}Ni_xMo_yCu_z$ alloys (t_a = 5 s); (f) The H_c vs. T_a plot of nanocrystalline $Fe_{82}Si_{3.6}B_{8.4}P_{3.6}Ni_{1.0}Mo_{0.4}Cu_1$ (Ni1) and $Fe_{81.5}Si_{3.6}B_{8.4}P_{3.6}Ni_{1.5}Mo_{0.4}Cu_1$ (Ni1.5) alloys for t_a = 5 s and 60 s.

melting the mixtures of Fe (99.99% pure), Si (99.99% pure), B (99.99% pure), Ni (99.9% pure), Mo (99.95% pure), Cu (99.99% pure), and Fe_3P (99.5% pure) in an argon atmosphere. Amorphous ribbons (thickness ≈ 20 μm, width = ~1.0 mm or ~5.0 mm) were prepared by a single roller melt spinner operated under a circumferential speed of 40 m/s. Calorimetry experiments were conducted by a differential scanning calorimeter (NETZSCH DSC 404C) at a heating rate of 0.33 K/s in an argon gas flow. The microstructure of the samples was characterized by X-ray diffraction (XRD, Bruker D8 Focus) with Cu K_α radiation and transmission electron microscopy (TEM, FEI Talos F200). The mean grain size (D) was estimated by manual measurement from the dark field TEM images. The saturation magnetic induction (B_s) of samples was measured by a vibrating sample magnetometer (VSM, Lake Shore 7410) under a maximum applied field of 800 kA/m. The coercivity (H_c) of samples was measured using DC B-H loop tracers (Rikken Denshi BHS-40S and Linkjoin MATS-2010SD). The permeability of nanocrystalline ribbons was measured by an impedance analyzer (Wayne Kerr 6500 B) at 1 kHz and 0.4 A/m. More details about sample preparation, heat treatment process, and magnetic properties measurement are presented in the Supplementary Materials.

The alloy design was started from a $Fe_{84}Si_4B_{8.4}P_{3.6}$ alloy, which has good glass-forming ability and a B_s of 1.83 T after nanocrystallization. The microalloying elements were added to the original Fe-Si-B-P alloy in an order of Ni, Mo, and Cu. Fig. 1a presents the XRD patterns of as-spun ribbons in this work acquired from their free-side. The thickness of ribbons prepared for this study is about 20 ± 2 μm for maintaining a constant cooling rate. A typical diffused peak for Fe-based amorphous alloys is confirmed for all Cu-free alloys, representing a good GFA. A bcc-Fe (110) peak is observed from the XRD patterns of Cu-containing ribbons, indicating the surface crystallization due to the deterioration in

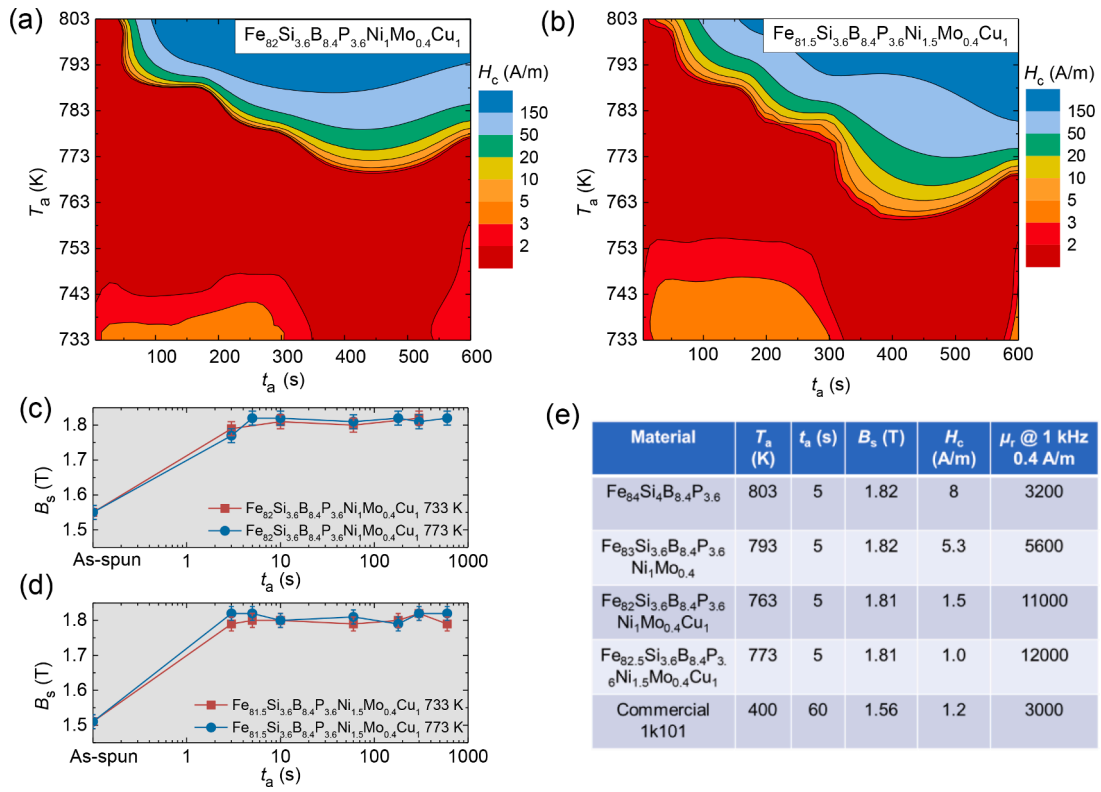

(e)

Material	T_a (K)	t_a (s)	B_s (T)	H_c (A/m)	μ_r @ 1 kHz 0.4 A/m
$Fe_{84}Si_4B_{8.4}P_{3.6}$	803	5	1.82	8	3200
$Fe_{83}Si_{3.6}B_{8.4}P_{3.6}Ni_1Mo_{0.4}$	793	5	1.82	5.3	5600
$Fe_{82}Si_{3.6}B_{8.4}P_{3.6}Ni_1Mo_{0.4}Cu_1$	763	5	1.81	1.5	11000
$Fe_{82.5}Si_{3.6}B_{8.4}P_{3.6}Ni_{1.5}Mo_{0.4}Cu_1$	773	5	1.81	1.0	12000
Commercial 1k101	400	60	1.56	1.2	3000

Fig. 2. (a) The H_c contour of Ni1 alloy annealed at different T_a and t_a; (b) The H_c contour of Ni1.5 alloy annealed at different T_a and t_a; (c) B_s of nanocrystalline Ni1 alloy annealed at $T_a = 733$ K and 773 K for different t_a; (d) B_s of nanocrystalline Ni1.5 alloy annealed at $T_a = 733$ K and 773 K for different t_a; (e) The soft magnetic properties of $Fe_{84}Si_4B_{8.4}P_{3.6}$, $Fe_{84}Si_{3.6}B_{8.4}P_{3.6}Ni_1Mo_{0.4}$, Ni1, and Ni1.5 nanocrystalline alloys and stress-relaxed commercial amorphous alloy 1k101.

GFA by Cu addition. We first optimized the amount of Ni alloyed to the original Fe-Si-B-P alloy. Fig. 1b shows the change in B_s and H_c for optimally annealed nanocrystalline $Fe_{84-x}Si_4B_{8.4}P_{3.6}Ni_x$ alloys. Although a few literatures indicated that adding Ni to Fe-based nanocrystalline alloys would reduce the B_s [17,25,26], our result suggests that the B_s of $Fe_{84-x}Si_4B_{8.4}P_{3.6}Ni_x$ alloys remains a constant when $x \leq 1.5$. The H_c decreases monotonically with the increasing Ni content, which coincides to the literatures [25,26]. Namely, replacing 1–1.5 at.% of Fe by Ni could make the GFA and H_c of $Fe_{84}Si_4B_{8.4}P_{3.6}$ alloy improved without sacrificing its B_s. Therefore, we selected $Fe_{83}Si_4B_{8.4}P_{3.6}Ni_1$ and $Fe_{82.5}Si_4B_{8.4}P_{3.6}Ni_{1.5}$ as ideal compositions for further microalloying Mo and Cu.

Previous study showed that replacing Fe by Mo could improve the soft magnetic properties but significantly reduce the B_s of Fe-based nanocrystalline alloys [27]. For our work, we tried to replace Si by Mo as we thought this may have less impact on B_s than replacing Fe. The effect of Mo addition on the B_s and H_c of optimally annealed $Fe_{83}Si_{4-y}B_{8.4}P_{3.6}Ni_1Mo_y$ alloys is presented in Fig. 1c. The H_c of nanocrystalline $Fe_{83}Si_{4-y}B_{8.4}P_{3.6}Ni_1Mo_y$ alloys is only slightly improved when $y = 0.4$. Further increasing the Mo content makes the H_c increase accompanied with a rapid decrease in B_s, which is obviously unwanted. Besides the influences on soft magnetic properties, Mo can facilitate the primary crystallization onset and suppress the secondary crystallization onset (Fig. 1d), which reflects the broadening of processing temperature window for nanocrystallization. Therefore, $Fe_{82.5-83}Si_{3.6}B_{8.4}P_{3.6}Ni_{1-1.5}Mo_{0.4}$ alloys were assessed as the optimum compositions among $Fe_{84-x}Si_{4-y}B_{8.4}P_{3.6}Ni_xMo_y$ alloys. The Cu-free alloy compositions show $B_s = 1.82 \pm 0.02$ T ($\rho = 7.48 \pm 0.01$ g/cm^3, $M_s = 194 \pm 2$ emu/g), $H_c = 5.3 \pm 0.5$ A/m, and relative permeability $\mu_r = 5600$ at 1 kHz and 0.4 A/m after nanocrystallization.

After determining the optimum Ni and Mo contents, 1 at.% Cu was added to the $Fe_{84-x}Si_{4-y}B_{8.4}P_{3.6}Ni_xMo_y$ alloys to further reduce its H_c and improving μ_r. Cu addition is a mixed blessing for Fe-based nanocrystalline alloys. On one hand, Cu significantly reduces the GFA of Fe-based alloys and can easily result in unexpected quench-in crystals in the amorphous precursors with high Fe content, e.g., the surface crystallization revealed in Fig. 1a. The presence of large surface crystals in amorphous precursors can deteriorate the soft magnetic properties of high-B_s nanocrystalline alloys [28]. On the other hand, proper Cu addition can introduce abundant nucleation sites to Fe-based nanocrystalline alloys, which greatly refines their microstructure [7,14,29]. Fig. 1f shows that 1 at.% Cu addition can reduce the optimum H_c of $Fe_{84-x}Si_4B_{8.4}P_{3.6}Cu_x$ alloys from 8.0 A/m to 1.9 A/m. Microalloying Ni and Mo together with Cu further reduces the H_c of nanocrystalline alloys slightly, while significantly broadening the temperature window that the optimum H_c can be achieved. $Fe_{81.5-2}Si_4B_{8.4}P_{3.6}Ni_{1-1.5}Mo_{0.4}Cu_1$ alloys in Fig. 1e shows slightly lower optimum H_c than the $Fe_{83}Si_4B_{8.4}P_{3.6}Cu_1$ alloy but their H_c remains at the optimum level (i.e., $H_c \leq 2$ A/m) for a much wider T_a range. $Fe_{81.5-2}Si_4B_{8.4}P_{3.6}Ni_{1-1.5}Mo_{0.4}Cu_1$ are also the optimum alloy compositions designed in this work.

Fig. 1f shows the soft magnetic properties of nanocrystalline $Fe_{82}Si_{3.6}B_{8.4}P_{3.6}Ni_{1.0}Mo_{0.4}Cu_1$ (Ni1) and $Fe_{81.5}Si_{3.6}B_{8.4}P_{3.6}Ni_{1.5}Mo_{0.4}Cu_1$ (Ni1.5) alloys with different annealing conditions. Although there is a crystalline feature presented on the XRD pattern of the free-side of ribbons, the lowest H_c of Ni1 alloy can reach 1.5 A/m at annealing temperature $T_a = 763$ K and annealing time $t_a = 5$ s. A low $H_c \leq 2$ A/m could be maintained for $T_a = 733$–783 K and $t_a = 5$ s, indicating a good stability of the low H_c in Ni1 alloy against the annealing temperature change. When t_a increases to 60 s, the lowest H_c for Ni1 alloy remains unchanged. The annealing temperature window for $H_c \leq 2$ A/m narrows down to 743–773 K, but the H_c is still ≤ 2.5 A/m at $T_a = 733$ K and 783 K for $t_a = 60$ s. This reflects a good stability of the low H_c for Ni1 alloy against annealing time change. The contour in Fig. 2a shows the stability of H_c for nanocrystalline Ni1 alloy against the variation of annealing conditions. The H_c remains below 3 A/m when the Ni1 alloy is annealed within a wide temperature window up to 50 K (733–783 K) at a wide time window of 5–600 s. Within the processing window that yields the

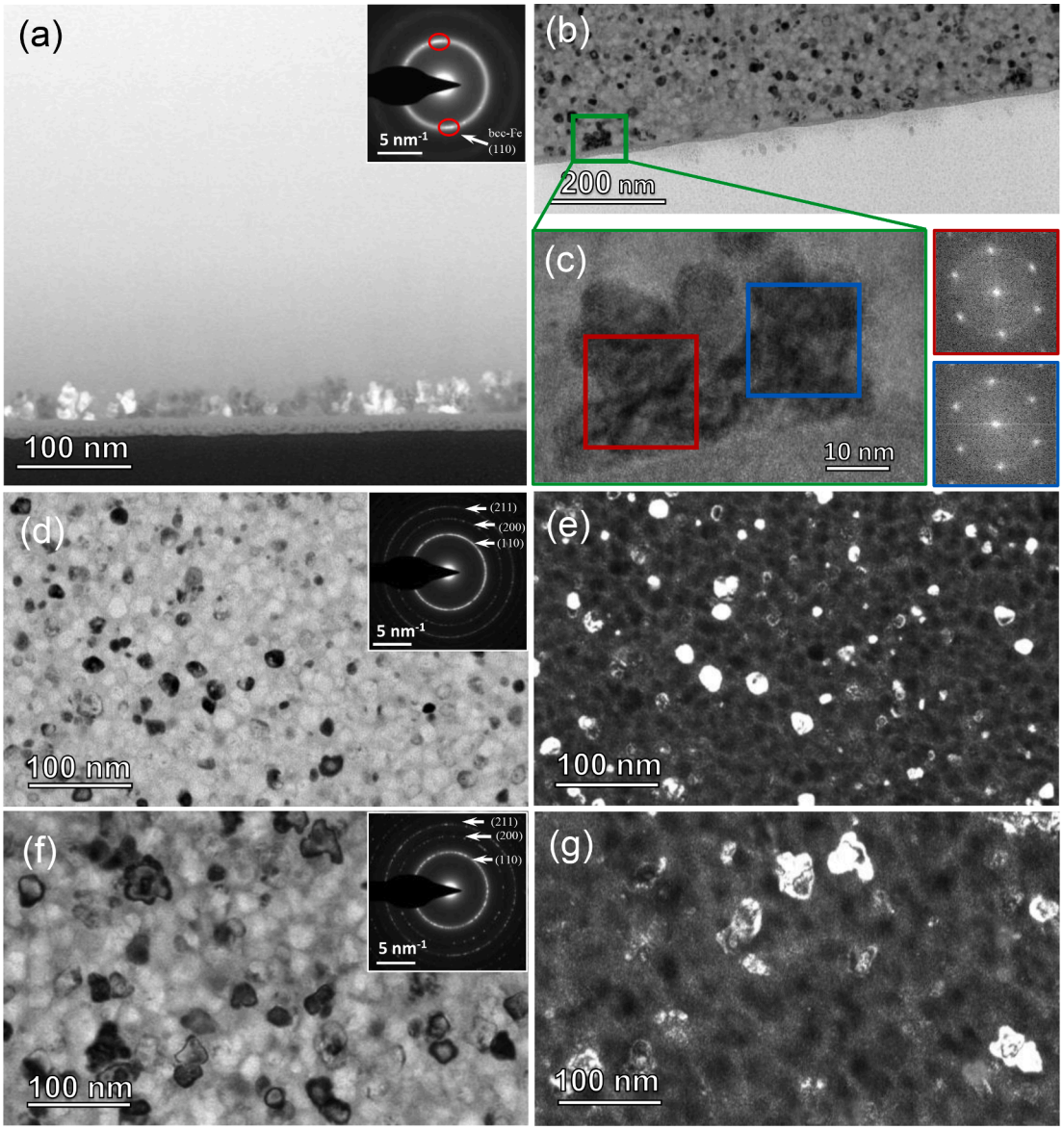

Fig. 3. (a) The DF4 image of the free side surface of as-spun $Fe_{82}Si_{3.6}B_{8.4}P_{3.6}Ni_{1.0}Mo_{0.4}Cu_1$ alloy, the inset shows the SAED pattern; (b) the bright field image of the free side surface of optimal annealed $Fe_{82}Si_{3.6}B_{8.4}P_{3.6}Ni_{1.0}Mo_{0.4}Cu_1$ alloy; (c) The HRTEM image of the large surface crystal green-circled in (b) and the FFT of the red and blue circled area in (c), the inset shows the SAED pattern; (d) The bright field image of the bulk region of optimal annealed $Fe_{82}Si_{3.6}B_{8.4}P_{3.6}Ni_{1.0}Mo_{0.4}Cu_1$ alloy, the inset shows the SAED pattern; (e) The dark field image of (d); (f) The bright field image of the bulk region of optimal annealed $Fe_{84}Si_4B_{8.4}P_{3.6}$ alloy, the inset shows the SAED pattern; (g) The dark field image of (f).

low H_c, the B_s of $Fe_{82}Si_{3.6}B_{8.4}P_{3.6}Ni_{1.0}Mo_{0.4}Cu_1$ alloy is kept stably at 1.81 ± 0.02 T ($\rho = 7.52 \pm 0.01$ g/cm^3, $M_s = 192 \pm 2$ emu/g) as shown by Fig. 2c.

As for the nanocrystalline Ni1.5 alloy, it has a slightly lower optimum H_c (1 A/m) than Ni1 while annealed for 5 s (Fig. 1f). The Ni1.5 alloy has a broader T_a window (733–803 K) to achieve the optimum H_c (≤ 2 A/m) than the Ni1 alloy. This alloy shows higher sensitivity to t_a compared with the Ni1 alloy. When t_a increases to 60 s, its optimum H_c slightly increases to the similar level as the Ni1 alloy (1.5 A/m). The T_a window for $H_c \leq 2$ A/m also narrows down to 753–793 K. The low H_c of Ni1.5 alloy is also accompanied with a high B_s of 1.81 ± 0.02 T (Fig. 2d). The processing window for Ni1.5 alloy to get $H_c \leq 3$ A/m is shown by the contour in Fig. 2b, which is $T_a = 733$–763 K, $t_a = 300$–600 s, and $T_a = 743$–783 K, $t_a = 5$–300 s. In Fig. 2e, we summarize the properties of different nanocrystalline alloys studied in this work heat treated by rapid annealing for 5 s. Since the permeability values were measured using a solenoid instead of a toroidal sample, it should be underestimated due to the demagnetizing effect. Thus, a commercial Fe-based amorphous product 1k101 were purchased and characterized after stress relaxation for comparison. The Ni1 and Ni1.5 alloys show relative permeability values beyond 10,000 at $f = 1$ kHz and $H = 0.4$ A/m, which are significantly higher than that of stress relaxed commercial 1k101 amorphous alloy.

The low coercivity and high permeability of nanocrystalline $Fe_{81.5–82}Si_{3.6}B_{8.4}P_{3.6}Ni_{1.0–1.5}Mo_{0.4}Cu_1$ alloys comes from their ultra-fine microstructure. The DF4 image in Fig. 3a indicates that there is a crystallite layer on the free side surface of as-spun $Fe_{82}Si_{3.6}B_{8.4}P_{3.6}Ni_{1.0}Mo_{0.4}Cu_1$ alloy. The size of these surface crystals could reach ~28 nm. In nanocrystalline $Fe_{81.5–82}Si_{3.6}B_{8.4}P_{3.6}Ni_{1–1.5}Mo_{0.4}Cu_1$ alloys, large dark features are found on the free side surface as shown by Fig. 3b. These features, for example the green circled one with 27 × 54 nm size, are proved to be single bcc-Fe grains by their identical Fast Fourier Transform (FFT) patterns for different regions calculated from the high-resolution TEM (HRTEM) image (Fig. 3c). The bulk region of the

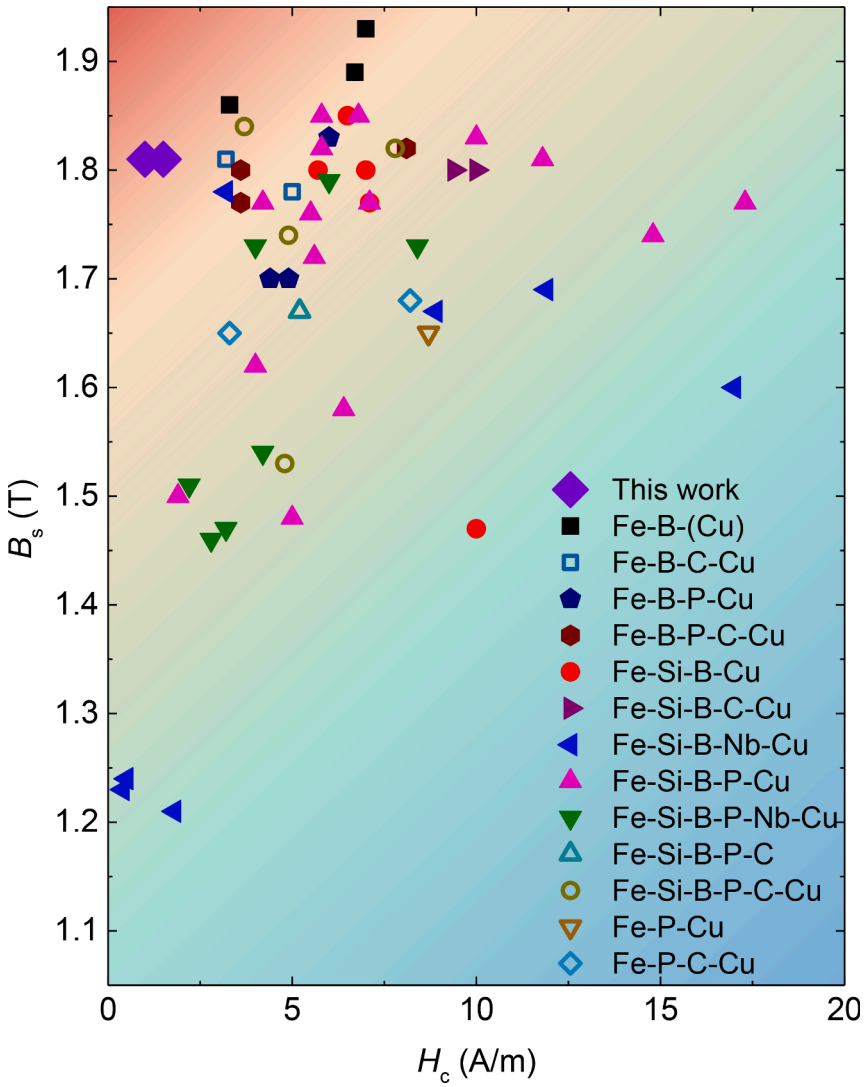

Fig. 4. The H_c vs. B_s plot of optimal annealed nanocrystalline alloys in this study and other Co-free Fe-based nanocrystalline alloys from literatures, the sources of the data are provided in the Supplementary Materials.

nanocrystalline $Fe_{82}Si_{3.6}B_{8.4}P_{3.6}Ni_1Mo_{0.4}Cu_1$ sample is free of these large grains and only shows homogeneously distributed round bcc-Fe grains with a mean size of 13.1 nm (Fig. 3d and e). For the original $Fe_{84}Si_4B_{8.4}P_{3.6}$ alloy before microalloying, the nanocrystalline microstructure in Fig. 3f and g is less homogeneous with a much larger mean grain size of 28.5 nm due to the presence of local large grains with irregular shapes. The existence of local large grains is not rare in Fe-based nanocrystalline alloys (e.g., $Fe_{77}Si_{10+x}B_{9-x}Nb_2Cu_1Al_1$ [30], $Fe_{85}Si_2B_8P_4Cu_1$ [31], etc.). The dramatic reduction in mean grain size and the absence of local large grains in $Fe_{82}Si_{3.6}B_{8.4}P_{3.6}Ni_1Mo_{0.4}Cu_1$ reflects that proper co-alloying Ni, Mo, and Cu significantly increases the number density of nucleation in the nanocrystallization process of $Fe_{81.5–82}Si_{3.6}B_{8.4}P_{3.6}Ni_{1.0–1.5}Mo_{0.4}Cu_1$ alloys. Due to the explosive nucleation in $Fe_{81.5–82}Si_{3.6}B_{8.4}P_{3.6}Ni_{1.0–1.5}Mo_{0.4}Cu_1$ alloys, the grain coarsening effect inherited from the surface crystals is strictly limited to a single layer (~30 nm) on the free side surface, which is minor compared with the overall ribbon thickness (~20 μm). Thus, nanocrystalline $Fe_{81.5–82}Si_{3.6}B_{8.4}P_{3.6}Ni_{1.0–1.5}Mo_{0.4}Cu_1$ alloys developed from amorphous precursors with 28 nm surface crystals still show a low $H_c \leq$ 2 A/m within a wide range of T_a and t_a. For industries, purity of raw materials is often lower than laboratories, and the precision of temperature and time control is usually less. The insensitivity of $Fe_{81.5–82}Si_{3.6}B_{8.4}P_{3.6}Ni_{1.0–1.5}Mo_{0.4}Cu_1$ alloys to slight surface crystallization and annealing conditions is beneficial for mass production.

The thermal history and structural features accumulated in an amorphous alloy could be inherited to the crystallization process [21,32-34]. The reduced GFA of high-B_s ($\geq$ 1.8 T) Fe-based nanocrystalline alloys often leads to a poor quality of the amorphous precursors, which deteriorates the soft magnetic properties of nanocrystalline alloys. Using ultra-rapidly quenched amorphous precursors (thickness $\approx$ 10 μm) that remain a more chaotic structure accompanied with high heating rate annealing is an effective way to develop ultra-fine microstructures with good magnetic softness ($H_c = 3 – 7$ A/m) in high-B_s alloy systems [17–20]. Soft magnetic properties of nanocrystalline alloys processed by this method may be sensitive to the annealing conditions [17,18,24]. In this work, we developed new nanocrystalline alloys by proper co-alloying Ni, Mo, and Cu to a Fe-Si-B-P alloy. This co-alloying method by Ni, Mo, and Cu induces plenty of nucleation sites in the nanocrystallization process and effectively limited the grain coarsening effect from surface crystals. Besides, it effectively reduces the sensitivity of new nanocrystalline alloys to the annealing conditions in the high heating rate annealing process. The resultant $Fe_{81.5–82}Si_{3.6}B_{8.4}P_{3.6}Ni_{1.0–1.5}Mo_{0.4}Cu_1$ alloys show an exceptional low H_c of 1–2 A/m, which is the lowest among a few nanocrytalline alloys whose $B_s \geq$ 1.8 T (Fig. 4). Such good soft magnetic properties can be developed from 20-μm-thick amorphous precursors

with 28-nm-large surface crystallites. The abovementioned properties are almost unchanged within a 40–50 K variation in T_a and a up to 600 s variation in t_a. The materials designed in this work show a more advanced combination of soft magnetic properties among the Co-free Fe-based nanocrystalline alloys reported in literatures (Fig. 4). In addition, the low sensitivity of its soft magnetic properties to surface crystallites and annealing conditions makes them more valuable in mass production.

In this paper, new $Fe_{84-x-z}Si_{4-y}B_{8.4}P_{3.6}Ni_xMo_yCu_z$ nanocrystalline soft magnetic alloys are designed by co-alloying Ni, Mo, and Cu to a Fe-Si-B-P alloy. The structural and magnetic properties of nanocrystalline $Fe_{84-x-z}Si_{4-y}B_{8.4}P_{3.6}Ni_xMo_yCu_z$ alloys are investigated. There are three noteworthy outcomes from this report as follows:

1) Minor addition of Ni ($\leq$ 1.5 at%) to Fe-based nanocrystalline alloys could reduce the H_c without sacrificing the B_s.
2) Proper co-alloying Ni, Mo, and Cu to a Fe-Si-B-P alloy can greatly increase the number density of nucleation in nanocrystallization process. This suppresses the formation of large, agglomerated grains inside the sample and the growth of those induced by surface crystallization. The average grain size decreases from 28.5 nm to 13.1 nm.
3) An exceptional low H_c of 1–2 A/m, high relative permeability μ_r beyond 10,000 at 1 kHz and 0.4 A/m, and high B_s of 1.81 T are achieved in the nanocrystalline $Fe_{81.5-82}Si_{3.6}B_{8.4}P_{3.6}Ni_{1-1.5}Mo_{0.4}Cu_1$ alloys.
4) The co-alloying of Ni and Cu significantly broadens the annealing temperature and time window for nanocrystalline alloys to remain excellent H_c and B_s. The optimal annealing temperature window is about 40–50 K with a time window up to 600 s.

Declaration of Competing Interest

The authors declare that they have no known competing financial interests or personal relationships that could have appeared to influence the work reported in this paper.

Acknowledgment

The authors thank the financial supports from National Natural Science Foundation of China (NSFC 52101205, 52271158, 92163108, 52231006), Zhejiang Province Key R&D Program (2022C01023).

Supplementary materials

Supplementary material associated with this article can be found, in the online version, at doi:10.1016/j.scriptamat.2023.115666.

References

[1] J.M. Silveyra, E. Ferrara, D.L. Huber, T.C. Monson, Soft magnetic materials for a sustainable and electrified world, Science 362 (2018) 418.
[2] G. Herzer, Modern soft magnets: amorphous and nanocrystalline materials, Acta Mater. 61 (2013) 718–734.
[3] H. Li, Z. Lu, S. Wang, Y. Wu, Z. Lu, Fe-based bulk metallic glasses: glass formation, fabrication, properties, and applications, Prog. Mater. Sci. 103 (2019) 235–318.
[4] L. Hou, W. Yang, Q. Luo, X. Fan, H. Liu, B. Shen, High Bs of FePBCCu nanocrystalline alloys with excellent soft-magnetic properties, J. Non-Cryst. Solid. 530 (2020), 119800.
[5] L. Hou, X. Fan, Q. Wang, W. Yang, B. Shen, Microstructure and soft magnetic properties of FeCoPCCu nanocrystalline alloys, J. Mater. Sci. Tech. 35 (2019) 1655–1661.
[6] L. Shi, K. Yao, Composition design for Fe-based soft magnetic amorphous and nanocrystalline alloys with high Fe content, Mater. Des. 189 (2020), 108511.
[7] Y. Li, X. Jia, W. Zhang, Y. Zhang, G. Xie, Z. Qiu, J. Luan, Z. Jiao, Formation and crystallization behavior of Fe-based amorphous precursors with pre-existing alpha-Fe nanoparticles - Structure and magnetic properties of high-Cu-content Fe-Si-B-Cu-Nb nanocrystalline alloys, J. Mater. Sci. Tech. 65 (2021) 171–181.
[8] Y. Zhang, P. Sharma, A. Makino, Effects of minor precipitation of large size crystals on magnetic properties of Fe-Co-Si-B-P-Cu alloy, J. Alloy. Compd. 709 (2017) 663–667.
[9] X. Li, J. Zhou, L. Shen, B. Sun, H. Bai, W. Wang, Exceptionally high saturation magnetic flux density and ultralow coercivity via an amorphous-nanocrystalline transitional microstructure in an FeCo-based alloy, Adv. Mater. (2022), 22055863.
[10] G. Herzer, Grain structure and magnetism of nanocrystalline ferromagnets, IEEE Trans. Magn. 25 (1989) 3327–3329 (1989).
[11] G. Herzer, Soft magnetic nanocrystalline materials, Scr. Mater. 33 (1995) 1741–1756.
[12] K. Suzuki, J.M. Cadogan, Random magnetocrystalline anisotropy in two-phase nanocrystalline systems, Phys. Rev. B 58 (1998) 2730–2739.
[13] J.D. Ayers, V.G. Harris, J.A. Sprague, W.T. Elam, On the role of Cu and Nb in the formation of nanocrystals in amorphous $Fe_{73.5}Nb_3Cu_1Si_{13.5}B_9$, Appl. Phys. Lett 64 (1994) 974–976.
[14] J.D. Ayers, V.G. Harris, J.A. Sprague, W.T. Elam, H.N. Jones, On the formation of nanocrystals in the soft magnetic alloys $Fe_{73.5}Nb_3Cu_1Si_{13.5}B_9$, Acta Mater. 46 (1998) 1861–1874.
[15] K. Hono, D.H. Ping, M. Ohnuma, H. Onodera, Cu clustering and Si partitioning in the early crystallization stage of an $Fe_{73.5}Si_{13.5}B_9Nb_3Cu_1$ amorphous alloy, Acta Mater. 47 (1999) 997–1006 (1999).
[16] P. Sharma, X. Zhang, Y. Zhang, A. Makino, Competition driven nanocrystallization in high B_s and low core loss Fe-Si-B-P-Cu soft magnetic alloys, Scr. Mater. 95 (2005) 3–6.
[17] K. Suzuki, R. Parsons, B. Zang, K. Onodera, H. Kishimoto, A. Kato, Copper-free nanocrystalline soft magnetic materials with high saturation magnetization comparable to that of Si steel, Appl. Phys. Lett. 110 (2017), 012407.
[18] B. Zang, R. Parsons, K. Onodera, H. Kishimoto, A. Kato, A.C.Y. Liu, K. Suzuki, Effect of heating rate during primary crystallization on soft magnetic properties of melt-spun Fe-B alloys, Scr. Mater. 132 (2017) 68–72.
[19] R. Parsons, B. Zang, K. Onodera, H. Kishimoto, T. Shoji, A. Kato, K. Suzuki, Core loss of ultra-rapidly annealed Fe-rich nanocrystalline soft magnetic alloys, J. Magn. Magn. Mater. 476 (2019) 142–148.
[20] R. Parsons, K. Suzuki, Nanocrystalline soft magnetic materials produced by continuous ultra-rapid annealing (CURA), AIP Adv. 12 (2022), 035316.
[21] B. Zang, L. Song, R. Parsons, J. Shen, M. Gao, Y. Zhang, J. Huo, Y. Sun, F. Li, K. Suzuki, J. Wang, W. Wang, Influence of thermal history on the crystallization behavior of high-B_s Fe-based amorphous alloys, Sci. China Phys. Mech. 66 (2023), 2561112.
[22] B. Zang, R. Parsons, K. Onodera, H. Kishimoto, T. Shoji, A. Kato, J.S. Garitalnandia, A.C.Y. Liu, K. Suzuki, Nanostructural formation kinetics in an Fe86B14 soft magnetic alloy investigated by in situ transport measurements under isothermal conditions, Phys. Rev. Mater. 4 (2020), 033404 (2020).
[23] K. Onodera, K. Suzuki, R. Parsons, B. Zang, Method for producing soft magnetic material, PCT/JP2017/028128.
[24] R. Parsons, B. Zang, K. Onodera, H. Kishimoto, T. Shoji, A. Kato, K. Suzuki, Nanocrystallisation and magnetic softening in Fe-B binary alloys induced by ultra-rapid heating, J. Phys. D: Appl. Phys. 51 (2018), 415001.
[25] X. Jia, Y. Li, L. Wu, W. Zhang, A study on the role of Ni content on structure and properties of Fe-Ni-Si-B-P-Cu nanocrystalline alloys, J. Alloy. Compd. 822 (2020), 152784.
[26] Z. Li, R. Parsons, B. Zang, H. Kishimoto, T. Shoji, A. Kato, J. Karel, K. Suzuki, Dramatic grain refinement and magnetic softening induced by Ni addition in Fe-B based nanocrystalline soft magnetic alloys, Scr. Mater. 181 (2020) 82–85.
[27] X. Jia, Y. Li, G. Xie, T. Qi, W. Zhang, Role of Mo addition on structure and magnetic properties of $Fe_{85}Si_2B_8P_4Cu_1$ nanocrystalline alloy, J. Non-Crystal. Solid. 481 (2018) 590–593.
[28] T. Liu, A. He, F. Kong, A. Wang, Y. Dong, H. Zhang, X. Wang, H. Ni, Y. Yang, Heterostructured crystallization mechanism and its effect on enlarging the processing window of Fe-based nanocrystalline alloys, J. Mater. Sci. Tech. 68 (2021) 53–60.
[29] X. Jia, B. Zhang, W. Zhang, Y. Dong, J. Li, A. He, R. Li, Direct synthesis of Fe-Si-B-C-Cu nanocrystalline alloys with superior soft magnetic properties and ductile by melt-spinning, J. Mater. Sci. Tech. 108 (2022) 186–195.
[30] Y. Sun, J. Li, L. Xie, A. He, Y. Dong, Y. Liu, C. Wang, K. Zhang, Effect of Si/B ratio on magnetic properties and microstructure of FeSiBNbCuAl nanocrystalline alloys, J. Non-Crystal. Solid. 566 (2021), 120839.
[31] M. Nishijima, M. Matsuura, Y. Zhang, A. Makino, Observation of Cu nanometer scale clusters formed in $Fe_{85}Si_2B_8P_4Cu_1$ nanocrystalline soft magnetic alloy by a spherical aberration-corrected TEM/STEM, Phil. Mag. Lett. 95 (2015) 277–284.
[32] L. Song, M. Gao, W. Xu, J. Huo, J. Wang, R. Li, W. Wang, J.H. Perepezko, Inheritance from glass to liquid: beta relaxation depresses the nucleation of crystals, Acta Mater. 185 (2020) 38–44.
[33] J.E.K. Schawe, J.F. Löffler, Existence of multiple critical cooling rates with generate different types of monolithic metallic glasses, Nat. Commun. 10 (2019) 1337.
[34] Y. Xie, S. Sohn, M. Wang, H. Xin, Y. Jung, M.D. Shattuck, C.S. O'Hern, J. Schroers, J.J. Cha, Supercluster-coupled crystal growth in metallic glass forming liquids, Nat. Commun. 10 (2019) 915.